The Role of Extracellular Matrix Phosphorylation on Energy Dissipation in Bone

Stacyann Bailey[1], Grazyna E. Sroga[1], Betty Hoac[2], Orestis L. Katsamenis[3], Zehai Wang[4], Nikolaos Bouropoulos[5], Marc D. McKee[2,6], Esben S. Sorensen[7], Philipp J. Thurner[8], and Deepak Vashishth[1]

[1]Department of Biomedical Engineering, Center for Biotechnology and Interdisciplinary Studies, Rensselaer Polytechnic Institute, Troy, NY, USA.

[2]Faculty of Dentistry, McGill University, Montreal, QC, Canada.

[3]Faculty of Engineering and Physical Sciences, University of Southampton, Southampton, UK

[4]Department of Mechanical, Aerospace, and Nuclear Engineering, Rensselaer Polytechnic Institute, Troy, NY, USA.

[5]Department of Material Science, University of Patras, Patras, Greece

[6]Department of Anatomy and Cell Biology, Faculty of Medicine, McGill University, Montreal, QC, Canada.

[7] Department of Molecular Biology and Genetics, Aarhus University, Aarhus, Denmark

[8]Institute of Lightweight Design and Structural Biomechanics, Vienna University of Technology, Vienna, Austria.

Corresponding Author:

Deepak Vashishth, PhD

Professor of Biomedical Engineering

Rensselaer Polytechnic Institute

110 8th Street, Troy NY 12180, USA

Phone: 518-276-2296

Email: vashid@rpi.edu

Abstract

Protein phosphorylation, critical for cellular regulatory mechanisms, is implicated in various diseases. However, it remains unknown whether heterogeneity in phosphorylation of key structural proteins alters tissue integrity and organ function. Here, osteopontin phosphorylation level declined in hypo- and hyper- phosphatemia mouse models exhibiting skeletal deformities. Phosphorylation increased cohesion between osteopontin polymers, and adhesion of osteopontin to hydroxyapatite, enhancing energy dissipation. Fracture toughness, a measure of bone's mechanical competence, increased with *ex-vivo* phosphorylation of wildtype mouse bones and declined with *ex-vivo* dephosphorylation. In osteopontin deficient mice, global matrix phosphorylation level was not associated with toughness. Our findings suggest that phosphorylated osteopontin promotes fracture toughness in a dose-dependent manner through increased interfacial bond formation. In the absence of osteopontin, phosphorylation increases electrostatic repulsion, protein alignment, and interfilament distance leading to decreased fracture resistance. These mechanisms may be of importance in other connective tissues, and the key to unraveling cell-matrix interactions in diseases.

Introduction

In recent years, the role of extracellular matrix (ECM) proteins and their post-translational modifications (PTMs) in modulating cell activity, cell-matrix interactions, and biomineralization processes has sparked tremendous interest in different connective tissue biological systems. In particular, it has been postulated that different levels of phosphorylation of matrix proteins play a critical role in coordinating calcification processes in normally [1–6] and pathologically [7,8] mineralized bone tissues either independently and/or in combination with collagen. These phosphoproteins also accumulate at the interfaces found across bone's hierarchical levels [9–11], but it remains unclear as to how their phosphorylation levels influence the mechanical properties of bone. We have recently shown the importance of phosphorylation of ECM proteins in regulating bone quality. Global phosphorylation level varied between cortical and trabecular bone [12], declined with age, and was associated with an increase in age-related skeletal fragility [13].

Given the importance and incomplete understanding of how total phosphorylation levels, as well as the heterogeneity of phosphorylation observed for different bone matrix proteins, contribute to skeletal fragility, animal models provide a valuable resource to investigate this further. In particular, certain animal models recapitulate key metabolic and skeletal characteristics seen in humans displaying, for example, the phenotypes of major phosphate-handling diseases such as ***hypo***phosphatemia [14–16], ***hyper***phosphatemia [17], and hypophosphat***asia*** [18–20]. Hyp mice – the murine analog of X-linked hypophosphatemia (XLH) – display low serum phosphate and accumulation of osteopontin (OPN) [14], a well-known noncollagenous protein serving as a powerful inhibitor of mineralization, and a key determinant of bone's resistance to fracture. In contrast to Hyp mice, fibroblast growth factor 23-deficient

77 mice (*Fgf23*$^{-/-}$ mice) are hyperphosphatemic, but like the Hyp mice also show accumulation of
78 OPN [17]. Both of these phosphate handling disease models exhibit a soft-bone (osteomalacia)
79 phenotype and display decreased cortical area, thickness, and strength [21,22]. The
80 hypophosphatasia mouse model (*Alpl*$^{-/-}$ mice) displays mineralization deficiencies characterized
81 by rickets/osteomalacia as well as elevated levels of inorganic pyrophosphate (PPi). The *Alpl*$^{-/-}$
82 mice also show increased levels of phosphorylated OPN compared to wild type (WT) mice [19].
83 Interestingly, Opn KO mice also show elevated levels of PPi despite having more mineralized
84 osteoid than wildtype (WT) controls [18]. As such, it appears that OPN levels, and possibly its
85 phosphorylation status, contribute to impaired matrix mineralization and may play a role in
86 skeletal integrity in these models.

87 The degree of OPN phosphorylation has significant effects on its structure and physiological
88 function [23]. For example, osteoclast adhesion is increased with phosphorylation [24] and
89 correlates with the extent of bone resorption [25]. Hydroxyapatite (HA) crystal formation and
90 growth are inhibited by OPN in a dose-dependent manner [26], and dephosphorylation of OPN
91 abolishes the inhibitory effect of OPN on HA formation by at least 40-fold [25]. In addition to
92 bone resorption and mineralization, OPN has been shown to play a mechanical role in bone,
93 influencing its resistance to fracture [27–29]. The negatively charged phosphate groups of serine
94 and threonine residues on OPN bind to multivalent positive ions on hydroxyapatite, and this
95 interaction is part of a bonding/cohesion process that limits separation of mineralized collagen
96 fibrils during mechanical loading [30]. Also important in this bone-toughening process are large,
97 covalently crosslinked (by transglutaminase) networks formed between neighboring OPN
98 molecules and between OPN and other bone matrix proteins [31–33]. Networks of crosslinked
99 OPN polymers are abundantly present in bone, and may reside in the interfibrillar collagenous

matrix, at cell-matrix interfaces, and in interfacial cement lines [33,34] where they may be critical for maintaining the overall strength of bone tissue [31,35,36]. Analysis of different tissues revealed that phosphorylation of OPN is highly variable, and typically only some of the potential phosphorylation sites are occupied *in vivo* [37]. In fact, it is currently unknown how many of all available amino acid residues in mouse OPN are phosphorylated *in vivo* because the balance between the activities of protein kinases and phosphatases reflects the phosphorylation state of the protein. Importantly, the difference in phosphorylation status results in altered biological and mechanical responses. Considering the functional relevance of OPN phosphorylation, this PTM may be an important determinant of bone matrix quality and fragility.

In this study, we investigate the role of OPN phosphorylation on bone fracture. To execute this, we first demonstrate that in mouse models of impaired phosphate regulation and increased skeletal fragility, the level of OPN phosphorylation declines. Next, we captured the effects of phosphorylated OPN on bone fracture toughness (resistance to crack propagation and fracture) by developing methods to enzymatically phosphorylate and dephosphorylate WT and OPN-deficient mouse bones *ex vivo*, then measure the resultant change in their mechanical competence. In an effort to gain a better understanding of the various factors that contribute to the mechanical function of phosphorylated OPN in bone matrix, we then conducted atomic force microscopy-force spectroscopy (AFM-FS) experiments demonstrating the effect of pH, ion charges, and phosphorylation levels on the energy dissipation properties of the OPN network using simplified synthetic and physiologically relevant surfaces. Based on these results, we propose that for appropriate mechanical function of bone, the phosphorylation status of OPN promotes fracture toughness up to a beneficial point. Phosphorylation or dephosphorylation

alters the interaction between charged groups on OPN, and between OPN and bone mineral leading to increased or decreased energy dissipation.

Results

Evidence of decreased osteopontin phosphorylation in mouse models of impaired phosphate metabolism and decreased mechanical properties

We first investigated whether the phosphorylation state of OPN varied using *in vivo* mouse models having phosphate disorders and known skeletal pathology linked to soft osteomalacic bones. Mineral-bound proteins were extracted from long bones of WT, Hyp, and *Fgf23*$^{-/-}$ mice. Total protein was quantified using a colorimetric detection system. From each sample, 2 µg of protein extract was loaded onto a 4-20% gradient SDS PAGE gel. Since the vast majority of OPN phosphorylation occurs at serine residues, we performed immunoblotting for phosphoserine in the mineral-binding protein extracts. In the bone matrix of both Hyp and *Fgf23*$^{-/-}$ mice, we found that mineral-bound OPN increased **(Figure 1a)** but global phosphorylation decreased **(Figure 1b)** as compared to WT controls. In addition, the post-immunoprecipation results show that despite the accumulation of OPN in Hyp and *Fgf23*$^{-/-}$ mice **(Figure 1c)**, the proportion of phosphorylated OPN was reduced compared to the bone of WT mice **(Figure 1d).** Given that these models have opposite levels of serum phosphate deviation from normal (hypophosphatemic vs. hyperphosphatemic), and display a reduction in bone strength [21,22,38,39] which may be dependent on defective mineralization but driven by the mineral-inhibiting protein OPN, our results suggest that osteopontin phosphorylation may be an important contributor to the fracture resistance of bone.

Phosphorylation status of osteopontin influences bone fracture toughness

To capture the effects of OPN phosphorylation on bone fracture toughness, we performed separate *ex vivo* phosphorylation and dephosphorylation of whole femurs from WT and Opn KO mice and subsequent mechanical testing. The global phosphorylation level in bone matrix increased in both genotypes with *ex vivo* casein kinase-II (CKII) phosphorylation (WT-*phosphorylated vs.* WT-*nonphosphorylated control, p=0.008;* Opn KO-*phosphorylated vs.* Opn KO-*nonphosphorylated control, p=0.007*) **(Figure 2a).** We observed a significant reduction in phosphoproteins with *ex vivo* dephosphorylation by alkaline phosphatase (WT-*dephosphorylated vs.* WT-*nondephosphorylated control, p=0.033;* Opn KO-*dephosphorylated vs.* Opn KO-*nondephosphorylated control, p=0.006*) **(Figure 3a).** Although the change in *ex vivo* phosphorylation between WT and Opn KO (delta-WT vs. delta-Opn KO **, Figure 2b**) was not statistically significant, we observed a significant difference in dephosphorylation between delta-WT and delta-Opn KO (**Figure 3b**), indicating that OPN-deficient bone can be modified to a greater extent than WT bone, likely attributable to increased permeability of enzymes into bones lacking OPN.

We observed higher fracture toughness with phosphorylation of WT bones (*WT-phosphorylated vs. WT-nonphosphorylated control, p=0.009*). In contrast, toughness declined in Opn KO mice following *ex vivo* phosphorylation (Opn KO-*phosphorylated vs.* Opn KO-*nonphosphorylated control, p=0.025)* indicating that phosphorylation of other bone matrix proteins in the absence of OPN did not improve the fracture resistance of bone **(Figure 4).** *Ex vivo* dephosphorylation caused a decrease in fracture toughness for the WT group (WT-*dephosphorylated vs.* WT-*nondephosphorylated control, p=0.012*) **(Figure 5)** while an increase

in fracture toughness was observed for Opn KO mice *(*Opn KO-*dephosphorylated vs.* Opn KO-*nondephosphorylated control, p=0.037).*

Energy dissipation of the osteopontin network is altered by levels of phosphorylation

We conducted atomic force microscopy-force spectroscopy (AFM-FS) studies using an *in vitro* experimental system to demonstrate that the phosphorylation status of OPN can affect bone toughness by altering energy dissipation. At pH 8.5, both OPN and hydroxyapatite (HA) surfaces are negatively charged. Under high Ca^{2+} concentration, the detachment energy increased more significantly as compared to H_2O and Na^+ environments. At pH 6.0 however, the protein and HA bear opposite charges. The slightly acidic pH lead to a moderate dissolution of HA over time, and therefore, it is expected that Ca^{2+} ions are present in solution from the beginning of the experiment. Further addition of Ca^{2+} ions decreased energy dissipation attributable to the reduction of sacrificial bond formation [42] (increase of effectively positively charged sites in OPN) as well as increased repulsion between OPN and HA. These results were also confirmed by the decline in energy dissipation that was observed for dephosphorylated OPN in Ca^{2+} solution at pH 7.4 as compared to native OPN, as well as dephosphorylated OPN in Na^+ solution at pH 7.4, all on mica substrates. Thus, the balance between Ca^{2+} ions in solution and the availability of negatively charged groups are both important for energy dissipation within the OPN network as well as at the OPN-HA interface. The results from AFM force spectroscopy are summarized in **Figure 6**.

Discussion

Extracellular bone matrix phosphoprotein osteopontin (OPN) has been recently implicated in disease models of ***hypo***phosphatemia [14–16], ***hyper***phosphatemia [17], and/or hypophosphat***asia*** [18–20]. Consistent with these studies, we observed full-length OPN in bone extracts of Hyp and *Fgf23*$^{-/-}$ mice. We further provide evidence that the phosphorylation level of OPN declined in these mouse models as detected by immunoblotting for OPN's phosphoserine residues. Given that these models display an aging-like skeletal phenotype [13] with impaired mineralization and osteomalacia, we considered whether the phosphorylation status of bone matrix proteins including OPN is an important determinant of their skeletal fragility. Our experimental model involved phosphorylation and dephosphorylation of both normal WT bones with OPN, and bones without OPN (Opn KO); thus, by comparing the change in fracture toughness caused by phosphorylation or dephosphorylation of the organic matrix between these two samples (WT-treated minus WT-control, delta-WT; and Opn KO -treated minus Opn KO -control, delta- Opn KO), the contribution of OPN phosphorylation alone can be isolated. Our results suggest that OPN and its phosphorylation level may be one of the dominant phosphoproteins in the determination of global bone matrix phosphorylation level and bone fracture toughness.

Fracture resistance of bone emerges from various mechanisms that exists at multiple length scales across bone hierarchy, and involves in part growth and packing of mineral foci into larger crossfibrillar aggregates such that the extracellular matrix becomes highly mineralized. In the context of the present work, at the nanoscale, major contributions to the intrinsic toughness of bone originate from the OPN-crosslinked protein networks [36,40] and the formation of dilatational bands involving osteocalcin (OC)-osteopontin complexes [29]. The OC-OPN complex has been recently shown to provide high shear toughness and ductility to the

interfibrillar interface [41]. Both the OPN-crosslinked protein networks and the OC-OPN complex presumably work together to control deformation and separation of mineralized collagen fibrils [42,43]. Here, we propose two co-existing mechanisms to elucidate how the addition or removal of phosphate groups on proteins, and particularly OPN, could affect bone mechanical function.

First, cation-mediated crosslinks are formed between two binding regions on one OPN polymer, multiple OPN polymers, and OPN and charged surface ions on HA (*e.g.*, Ca^{2+}, Na^{+}) **(Figure 6- figure supplement 3)** [44]. These salt-bridges are weak, but reformable sacrificial bonds that prevent portions of OPN polymers from rupturing (cohesion of the OPN meshwork) and debonding of OPN from HA during repetive mechanical loading [30,40,45]. The high affinity of OPN to Ca^{2+} ions was reinforced in our AFM-FS studies. We used bovine milk OPN as the model protein because of its natural and extensive phosphorylated status [46]. In the presence of Ca^{2+} ions and when both phosphorylated milk OPN and HA are negatively charged, detachment energy increased significantly. The increase in detachment energy was also observed between OPN and mica substrate **(Figure 6).** Ca^{2+}-mediated crosslinks were also formed between OPN polymers, which increased cohesion of the OPN meshwork, indicated by higher detachment energy **(Figure 6- figure supplement 2)**, which is generally associated with loading of multiple molecules in parallel [47]. Thus, via the effects mentioned above the meshwork is able to stretch more and increase the energy required for complete detachment. Dephosphosphorylation of milk OPN or reversing the charge on HA both resulted in decreased energy dissipation **(Figure 6).** Similarly, phosphorylation of WT bone specimens *ex-vivo* under our experimental conditions caused an approximate 18% increase in fracture toughness **(Figure 4a)** whereas, dephosphorylation decreased toughness by 25% **(Figure 5a).** These results suggest

232 that phosphorylation is enabling various matrix/mineral interactions, and hence, dissipating
233 energy.

234 Second, phosphorylation can alter protein network conformation, the mechanical behavior of
235 the organic matrix, and consequently the macroscopic fracture toughness of bone [10,40,48]. A
236 recent experimental study [49] demonstrated that intrinsically disordered proteins (IDPs) and
237 their phosphorylation status can alter neurofilament protein alignment and distance between
238 filaments, resulting in changed energy dissipation of the network **(Figure 7).** Neurofilaments are
239 a valuable model system for examining phosphorylation-driven interactions of IDPs owing to
240 their high modularity in protein content and phosphorylation levels. Both collagen and
241 neurofilaments are bundled network systems that interact with IDPs [50,51]. For example, non-
242 collagenous proteins in bone matrix such as small integrin-binding ligand, N-linked
243 glycoproteins (SIBLINGs) are IDPs, interact with collagen, and gain more folded features when
244 post-translationally modified (phosphorylation, glycation, acetylation, sulfation, cleavage) [52].
245 In this regard, the SIBLING proteins (*e.g.*, osteocalcin, osteonectin, fibrillins, etc.) interacting
246 with collagen filaments/fibrils may be considered analogous to neurofilament proteins
247 [50,53,54]. Our AFM-FS studies showed that in the presence of excess Ca^{2+} ions strong
248 cohesion and excessive crosslinking of the OPN meshwork reduces the stretching ability of the
249 meshwork, leading to shorter pulls, increased repulsion of all positive sites, which likely
250 increased distance in the meshwork, and diminished detachment energy. We postulate that the
251 increase in global phosphorylation of other bone matrix proteins in the absence of OPN (*e.g.*,
252 other SIBLING matrix proteins) may also potentially result in increased protein alignment and
253 larger interfilament distance between mineralized collagen fibrils, to a detrimental degree that

decreases matrix interaction, energy dissipation, and consequently fracture resistance in osteopontin deficient mice **(Figure 4).**

We observed a non-linear dose response relationship between the level of global matrix phosphorylation and bone fracture toughness in wildtype mice **(Figure 8a).** Phosphorylation explained ~36% of the variance in fracture toughness and this relationship was not observed in the absence of OPN **(Figure 8b).** Taken together, this data supports the previously mentioned mechanism involving increased interaction energy and sacrificial bond formation between OPN and HA as well as between OPN polymers. The AFM-FS studies show that adhesion is not only dependent on the charge of OPN and HA under a certain environment but also the availability of free Ca^{2+} ions. The remaining variance in fracture toughness may be associated with the formation of OC-OPN complexes or enzymatic OPN-crosslinked protein networks. It has been previously shown that crosslinking of OPN by transglutaminase-2 enzyme (TG2) increases interfacial adhesion and toughness [36]. However, OC inhibits TG2 crosslinking activity most likely by competing for the binding site on OPN [32]. As such, there is insufficient evidence at present that TG2 crosslinking of OPN and phosphorylation of OPN are independent. Although *ex vivo* phosphorylation of Opn KO mice bone decreased fracture toughness **(Figure 4a),** and dephosphorylation increased toughness compared to the respective untreated Opn KO mice bone **(Figure 5a)**, unlike WT, we did not observe an association between the level of global matrix phosphorylation and fracture toughness in these mice **(Figure 8b).** As noted above, excessive crosslinking can be detrimental to protein networks by increasing repulsion, interfilament distance, and stretching ability. This data suggests that although global matrix level of phosphorylation affects fracture toughness, the contribution of phosphorylated OPN may be critical in the determination of bone toughness.

Our current study is not devoid of limitations and we acknowledge other phosphorylation interactions that may potentially influence the outcomes. The gross skeletal phenotype of Opn KO mice is normal compared to WT mice [55,56]. However, increased mineralization was found in some areas of cortical bone [57], and the bones are mechanically weaker. The collagen structure in Opn KO mice was also shown to be highly disorganized which further causes disorganization of mineral [58]. OPN in bone resides at its surfaces (including lining the lacuno-canalicular system) in the thin structure known as the *lamina limitans* [9], and throughout bulk bone. Thus, its alterations *in vivo* may affect many processes including mineral binding [5], cell attachment as part of the bone remodeling cycle, cell signaling that may affect mechanosensation, and the structural integrity of bone. Our *ex vivo* experiments were conducted under physiological conditions to alter the organic matrix with buffer solutions containing magnesium chloride, calcium, and EDTA to prevent any alterations in mineral. The AFM measurements are not fully quantitative, but the potential lies in examining relative differences, as was done in this study. Also, by using the same cantilever, the measurements are very accurate and reproducible. Bovine milk OPN contains approximately 28 phosphorylation sites and all but a few residues in this motif are phosphorylated. The higher phosphorylation levels essentially allow for demonstration of the principal effects seen in whole-bone fracture toughness tests following increased phosphorylation. Attempts to over-phosphorylate bovine milk OPN (our source OPN) would likely be unsuccessful as the nonphosphorylated serine residues in bovine OPN are not located in recognition sequences of any specific kinase. The lack of experiments on OPN with a varying range of phosphorylation levels may be seen as a limitation, but nevertheless we provide data points for the most extreme cases, and, different from the physiological system, we control the concentration of Ca^{2+} ions.

Despite the fact that the maximum-load method for measuring fracture toughness demonstrates the least variability compared to other methods [59], there is inherent variability in fracture toughness tests. For example, we have shown with a larger sample size that Opn KO mice have lower fracture toughness compared to WT mice [28,29]. The data in Figures 4 and 5 are from a different set of control bones and fracture toughness values vary across bones from the same batch of mice attributable to inherent differences between animals, and because of variations in any mechanical testing method (including fracture toughness testing). Accordingly, we have minimized variations between animals by conducting pairwise comparison *i.e*. WT-dephosphorylated *vs* WT-controls. Such comparison, as noted above, also allows us to determine the contribution of OPN phosphorylation and dephosphorylation while accounting for compounding effects of other changes in the bone matrix.

In conclusion, this study shows for the first time that osteopontin and its phosphorylation level promotes fracture toughness of bone. The heterogeneity in osteopontin phosphorylation, alters interfacial adhesion and cohesion of the OPN meshwork leading to increased or decreased energy dissipation. In the absence of osteopontin, phosphorylation and de-phosphorylation of other bone matrix proteins impact bone toughness in a binary stepwise manner. We expect that our study holds the potential to begin understanding the need for regulation of global matrix phosphorylation and heterogeneity in phosphorylation for different proteins with respect to maintaining skeletal health and whose alterations influence bone fragility in diseases.

Materials and Methods

Key Resources Table				
Reagent type (species) or resource	**Designation**	**Source or reference**	**Identifiers**	**Additional information**
Genetic reagent (*M. musculus*)	C57BL/6NCrl	Charles River	RRID: IMSR_CRL:27	
Genetic reagent (*M. musculus*)	B6.Cg-*Phex*^{Hyp}/J	Jackson Laboratory	Cat#: 000528 RRID: IMSR_JAX:000528	Animals maintained in Dr M Mckee lab.
Genetic reagent (*M. musculus*)	*Fgf23*$^{-/-}$	PMID: 15579309		Animals were a gift from Dr. B. Lanske

Genetic reagent (*M. musculus*)	B6.129S6(Cg)-*Spp1*^{tm1Blh}/J	PMID: 9661074		Animals were a gift from Dr S. Rittling.
Genetic Reagent (*B. taurus*)	Milk protein (Mammary gland)	PMID: 8320368		Provided by Dr ES Sorensen
Chemical compound, drug	Synthetic hydroxyapatite	Androitis et al., 2010. Crystal Research and Technology		Produced by Dr N. Bouropoulos
commercial assay or kit	pIMAGO biotin HRP Detection	Tymora Analytical	Cat# 900-100	
antibody	anti-OPN (goat polyclonal)	R and D Systems	Cat# AF808, RRID: AB_2194992)	(1:100,000µL)
antibody	anti-phosphoserine (rabbit polyclonal)	Thermo Fisher Scientific	Cat# 61-8100, RRID: AB_2533940)	(1:2500µL)

Immunoprecipitation and immunoblotting for OPN in mouse models of phosphate disorder

Long bones from 6-week-old Hyp and *Fgf23*$^{-/-}$ mice (and WT age-, strain-, and sex-matched controls, n=3) were collected and bone proteins extracted as described previously [60]. In brief, cleaned frozen bone samples were pulverized, cooled in liquid nitrogen, and bone protein extracted from this powder twice at 4 °C for 24 hours with 4 M guanidium-HCl in 50 mM Tris-HCl, pH 7.4 containing protease and phosphatase inhibitors (0.1 mM phenylmethylsulfonyl fluoride (PMSF), 100 µg/mL of benzamidine, 5 µg/mL leupeptin, 1 mM sodium pyrophosphate, 1 mM β-glycerophosphate, 1 mM sodium orthovanadate, and 5 mM sodium fluoride). Mineral-bound proteins were then extracted twice at 4 °C for 24 hours with 0.5 M EDTA, 50 mM Tris-HCl, pH 7.4 containing protease and phosphatase inhibitors. The mineral-binding protein fraction was then concentrated and washed in 5 mM sodium bicarbonate, then quantified using the bicinchoninic acid protein assay (Pierce, Rockford, IL, USA).

For each sample, 10 µg of total mineral-bound bone protein extract was mixed with 300 µL of 100 mM sodium acetate, pH 5.5 containing 1 mM PMSF and 0.1 mM leupeptin and incubated on ice for 3 minutes, and then gently mixed with rotation at 4 °C for 10 minutes. Next, 10 µL of 0.2 mg/mL goat anti-mouse osteopontin antibody (R&D Systems, Cat# AF808-CF, Minneapolis, MN, USA) was added and samples were gently rotated at 4 °C for 1 hour, followed by the addition of 50 µL of Protein A/G PLUS-Agarose beads (Santa Cruz, SC-2003, Dallas, TX, USA) and gentle rotation at 4 °C for 1 hour. Samples were spun at 2000 × g for 1 minute, and

supernatants were removed. Beads were then washed in cold 100 mM sodium acetate buffer, pH 5.5 three times, and immunoprecipitated proteins were eluted in 2 × Laemmli protein loading buffer. Samples were resolved on a 4-20% gradient SDS-PAGE gel, transferred onto PVDF membranes and immunodetected using anti-mouse osteopontin (R&D Systems, Minneapolis, MN, USA) and anti-phosphoserine (Invitrogen, Cat# 61-8100, Carlsbad, CA, USA) antibodies. Two technical replicates were performed for *Fgf23*$^{-/-}$ mice and corresponding WT littermates experiments while four technical replicates were performed for the Hyp and corresponding WT littermates experiments.

In vitro phosphorylation and dephosphorylation of whole mouse bone

Sample Preparation

Previously frozen femora were dissected from twenty-eight six-month-old male Opn KO (n=14) and C57BL/6NCrl wild-type (WT, n=14) mice. The sample size reflects the number of independent biological replicates and were based on results from previous pilot studies and publications from the laboratory [12,29]. Bones were cleaned of soft tissue and femoral head and condyle removed for experimental uniformed treatment throughout the bone. A notch was created on the anterior side in the mid-shaft of all samples using a slow speed diamond blade saw and sharpened using a razor blade (IsoMet Low Speed Saw, Buehler) This method produces a sharp notch with a root radius of ~10 μm [59]. The crack length is defined in terms of the half crack angle and fracture toughness testing is accurate for half crack angles between 0-110 degrees [59]. A specimen was considered an outlier and removed if crack angles were larger than two standard deviations from the mean, and if notches were off-centered or extended greater than 1/3 of the cortex. Consistent with physiological loading, the anterior side was chosen so that the notch experiences tension during bending test. The notch represents a pre-existing crack that will initiate and propagate into a large-scale catastrophic fracture. The bones were then rinsed with 1 x phosphate buffered saline (PBS) and stored in saline soaked gauze at -80°C until use.

In vitro Phosphorylation and Dephosphorylation

One limb of each animal (left or right) was randomly selected for phosphorylation and the contralateral limb served as the non-phosphorylated control [Opn KO (n=7) and WT (n=7)]. Phosphorylation was conducted by incubating the samples for 48 hours at 30 ºC with casein kinase II (CK2) and the reaction buffer (New England BioLabs, Ipswich, MA). Adenosine triphosphate (ATP) (2 mM) was added to the buffer as the phosphoryl donor for CK2. The incubating solution also contained protease and phosphatase inhibitors (final concentration 2 x, Pierce Biotechnology, Rockford, IL), and antibiotics [ampicillin (100 μg/μL) and kanamycin (50 μg/μL)]. ATP, CK2, and antibiotics were also added second time to the reaction at the 20 hour of incubation. The non-phosphorylated samples (i.e. controls) were placed in a similar solution without added enzymes for the same time period and temperature.

In a different set of animals, one limb was randomly selected for de-phosphorylation and the contralateral limb served as the nondephosphorylated control [Opn KO (n=7) and WT (n=7)]. De-phosphorylation was conducted by incubating the samples for 48 hours at 37 ºC with calf

intestinal alkaline phosphatase (CIP) and the CIP reaction buffer (New England BioLabs, Ipswich, MA). In pilot and published studies [12] we did not observe increase in either phosphorylation or dephosphorylation of bone samples after 48h. The incubation solution also contained protease inhibitor and antibiotics as previously described. CIP enzyme was also added second time to the reaction at the 20 hour of incubation. The non-dephosphorylated samples (i.e. controls) were placed in a similar solution without added enzymes.

Mechanical Testing

All femora were scanned using micro-computed tomography (μCT) at 70 kVp, 114 mA, 200 ms integration time and at high resolution 10.5μm voxel size (vivaCT 40, Scanco Medical AG, Bassersdorf, Switzerland) for measuring bone geometry. Following in-vitro phosphorylation and dephosphorylation treatment, samples were loaded in three-point bending until failure at a loading rate of 0.001 mm/s (Elf Enduratec 3200). The resulting load displacement curve was used to calculate a single-valued fracture toughness K_c at maximum load for each sample [59]. Toughness measured here is dependent on the material reflecting the changes due to phosphorylation or dephosphorylation.

Protein Extraction, Quantification, and Phosphoprotein Detection

After mechanical testing, all bones were defatted, lyophilized (freeze-dried), and weighed (approximately 20-40 mg). Samples were then placed in eppendorf tubes with 600 μL of extraction buffer consisting of 0.05 M EDTA, 4 M guanidine chloride, and 30 mM Tris-HCl. The bones were subsequently homogenized, centrifuged, and the supernatant collected (Omni Inc, Kennesaw, GA). The supernatant from each sample was placed into a micro-dialysis vial and underwent simultaneous protein isolation and demineralization over two days at 4 °C, pH 7.4, against several changes of 1 x PBS and 5 mM EDTA.

The amount of protein in the samples was quantified using the Coomassie Plus (Bradford) Assay. The measurement of phosphorylated proteins was done using the pIMAGO-biotin Phosphoprotein Detection assay kit [12] (Tymora Analytical, West Lafayette, IN). Samples were tested in triplicates for each assay. Briefly, protein mixtures were bound to the wells by overnight incubation at 4 °C. After a series of washing and blocking, the wells were incubated with pIMAGO reagent for attachment of the nanopolymer to phosphate groups on proteins. The wells were washed again, incubated with avidin-HRP followed by the provided colorimetric-based detection system. The absorbance was read at 415 nm using a micro-plate reader (Infinite M200, Tecan). The amount of global protein phosphorylation was calculated as absorbance/ng of protein. Assays for protein concentration and phosphoprotein detection were ran in triplicates.

Data Analysis for Global Phosphorylation

The mean and standard deviation were calculated for total protein phosphorylation amount and fracture toughness. Paired samples t-test was used to compare differences between the groups (WT-*phosphorylated vs.* WT-*nonphosphorylated;* Opn KO-*phosphorylated vs.* Opn KO - *non phosphorylated*). Because phosphorylation modifies the organic matrix including OPN, we compared the change in fracture toughness caused by phosphorylation of the organic matrix with (WT-treated *minus* WT-control, delta-WT) and without osteopontin (Opn KO-treated *minus* Opn KO -control, delta- Opn KO) by independent samples t-test. The same analysis was done for

dephosphorylated samples and nondephosphorylated controls conducted on separate animals. All analyses were conducted using IBM SPSS 21 and two-tailed significance threshold set at 0.05 for both paired and independent samples t-test.

Atomic Force Microscopy - Force Spectroscopy Studies

Chemicals

All chemicals were purchased from Sigma-Aldrich® (Sigma-Aldrich Company Ltd., Gillingham, Dorset, UK) unless otherwise stated.

Preparation and Characterization of Hydroxyapatite (HA) Powder

Synthetic HA was produced for the functionalization of the AFM cantilever in order to simulate the mineralized fiber – NCP – mineralized fiber interaction. The preparation of the synthetic HA crystals was performed by the simultaneous addition of 250 ml aqueous solution of H_3PO_4 (0.3 M) and 250 ml aqueous solution of $CaCl_2 \cdot 2H_2O$ (0.5 M) to 500 ml ultrapure boiling water. To avoid temperature fluctuation, both reactants were added at a rate of approximately 2.5 mL per minute under continuous stirring. Prior and during the addition of the reactants, nitrogen gas was bubbled through the solution in order to remove the dissolved CO_2. At all times, the pH was kept between 9.0 and 10.0 by the addition of concentrated NH_4OH solution. Upon the completion of the addition, the solution was kept under stirring for 24 h at 80 °C before cooling to room temperature. To retrieve the HA crystals, the suspension was filtered through a 0.22 μm membrane filters (Whatman, Maidstone England). Finally, the crystals were dried and "matured" at 150 ^oC for 24 h and stored in a desiccator. The end product was characterized by means of X-Ray Diffraction (XRD), Fourier Transform Infrared Spectroscopy (FTIR) and Scanning Electron Microscopy equipped with Energy-dispersive X-ray analyser (SEM/EDX; Zeiss Supra 35VP). XRD analysis was performed using a standard powder diffractometer (Siemens D8) with Ni-filtered $CuKa_1$ radiation (λ = 0.154059 nm) and the acquired diffraction spectra were matched against JCPDS reference data using the EVA® XRD software. The FTIR spectra were acquired using an Excalibur® spectrophotometer (Digilab, Japan) at a resolution of 2 cm^{-1} using the KBr pellet method.

Preparation and Characterization of Hydroxyapatite (HA) Surfaces

HA surfaces were prepared through the "maturation" of CaP cements in Ringer solution as described previously [61,62]. In brief, the cements were made by mixing alpha-tricalcium phosphate (a-TCP) powder with 4.0 % w/v disodium hydrogen phosphate (Na_2HPO_4) solution at liquid (mL)/powder (g) ratio of 0.32, homogenized by a spatula for 1 min in agate mortar and then spread carefully on Silastic® M RTV Silicone Rubber moulds. The specimens were kept in 100% humidity for 12 h and then placed in 60 mL of Ringer's solution at 37 ^oC for 7 days to harden. During the maturation period, the a-TCP is transformed into calcium-deficient HA following the hydrolysis of the a-TCP according to the reaction $3Ca_3(PO_4)_2 + H_2O \rightarrow Ca_9(HPO_4)(PO_4)_5OH$ [63].

OPN Purification and Dephosphorylation

In bovine milk, OPN is subjected to proteolytic processing by proteinases such as thrombin [64], plasmin, cathepsin D or matrix metalloproteinases [65]. In this work isolated OPN from bovine milk as essentially described in [66]. The principal components are N-terminal OPN fragments ending between residues 145 and 153 of the mature protein as well as the mature full

length protein [67]. After isolation, OPN was stored in a desiccator at room temperature until use. Dephosphorylated milk OPN was prepared as described in [68]. Briefly, OPN was incubated with bovine alkaline phosphatase (ALP) (20 mU ALP/μg protein) in 10 mM ammonium bicarbonate (pH 8.5) overnight at 37 °C and subsequently analyzed by MALDI-TOF MS to verify dephosphorylation.

Buffer Solutions

The buffers used were the same as previous studies [24,44,45]. More specifically, Na Buffer (150 mM NaCl, 10 mM HEPES), Ca Buffer (40 mM $CaCl_2$, 110 mM NaCl, 10 mM HEPES) and ultra pure water (H_2O). Each solution was divided into separate vials and ph adjusted for each experiment using either HCl or concentrated NaOH solution.

Adsorption of OPN on Model Surfaces

The lyophilized OPN was dissolved in ultrapure water (concentration 2 μg/μl) and absorption of OPN film on the model surfaces (HA or mica) was accomplished using the "drying droplet" method. During this process, a small drop (4 μL) of OPN solution was deposited onto a freshly cleaned and dried HA or mica surface which was previously glued on the bottom of the fluid cell using 5 minute-setting epoxy. The droplet was then left to dry inside the AFM hood forming a thin protein film on the model surface, and then rehydrated with the appropriate solution.

AFM Cantilevers for Force Spectroscopy Measurements

One aggregate of synthetic HA crystals was glued to a tipless monolithic silicon AFM probe (AIO-TL, Budget Sensors) using epoxy glue (Araldixe®, Huntsman, The Woodlands, Texas, USA). For this, a few micrograms of the synthetic HA crystals were added in 5 mL of ethanol and stirred vigorously to produce a dispersion. At this stage, 500 μL of this dispersion were deposited onto a glass slide and left to dry. A droplet of epoxy was placed by the side of the dry crystals and the glass slide was placed into the AFM. The AFM probe was then engaged carefully onto the epoxy, pulled back, and engaged again on the aggregate of choice. After two minutes in contact, the probe was withdrawn and left in the AFM for an additional 30 minutes to ensure complete setting of the epoxy. An example of the end result is presented in Figure 6-figure supplement 1.

Force Spectroscopy Experiments

Force spectroscopy measurements of the adhesive properties of the OPN film under various ionic environments were conducted by means of an atomic force microscope (MFP3D, Asylum Research, Santa Barbara, CA, USA) using an open fluid cell setup. Following Fantner et al.'s protocol [44], all experiments were performed subsequently and at the same location. Exchange of solution, for altering the ionic environment and the pH, was carried using a syringe-pump inlet/outlet system without moving the head. In each environment, 50 -80 pulls were collected and analysed using a custom made Matlab® script (version 7.10.0.4999, The MathWorks Inc, Natick, Massachusetts, USA). For each force curve, the cantilever was positioned 3 μm away of the surface, driven in full contact with it, and after a dwell time of 10 sec was retracted back to the starting position. During these cycles, the approach and retraction velocities were set to 2.0 μm/sec and 5.0 μm/sec, respectively. Full contact was defined as the tip-sample repulsive force reaching a threshold value of 15 nN. The spring constant, k, of the cantilever probe was measured prior to the functionalization using the thermal noise method [59], and followed by the

Inverse Optical Lever Sensitivity (InvOLS) of the system. The later was determined by acquiring ten (10) force curves on a nominally infinitely stiff surface (*i.e*. the glass slide). A line was then fitted on the loading part of each force curve and the slope of the fitted line was used as the InvOLS. The mean InvOLS value of all ten curves was then used as the InvOLS of the cantilever. In the case of the HA-functionalised cantilevers the spring constant was reassessed using the thermal method post-functionalization and the resulting value was used for the analysis. Force spectroscopy measurements of phosphorylated/dephosphorylated OPN on mica surfaces were conducted using Olympus BL-RC150VB-C1 Bio-levers (Olympus Optical Co., Ltd., Tokyo, Japan); spring constant 6 pN/nm (0.006 N/m), while stiffer (c. 0.18 N/m) cantilevers were used for the HA experiments. Maximum force from force spectroscopy experiments are reported in Supplementary Files 3 and 4.

Data Processing and Analysis

All force curves were exported in ASCII (plain text files) and processed in Matlab®. Each force curve was split into its approaching and retraction parts (Figure 6- figure supplement 2). Energy dissipation was defined as the area enclosed by the retraction curve and the X-axis from the point of contact (X=0, Y=0) to the "Pulling Length"; where the latter was defined as the length from contact to the maximum distance at which the adhesion is smaller than the 1.0 % of the Maximum Force (maximum adhesion force registered during retraction, i.e the Y-minimum of the retraction curve). Statistical analysis was performed in Origin® (OriginPro version 9.0.0; OriginLab Corporation, Northampton, MA, USA). The normality of the distributions was assessed by means of a Kolmogorov-Smirnov test. Differences in Energy between the different environments were assessed by means of two-sided unpaired Student's t-test (significance threshold p =0.05).

Acknowledgements

This work was supported by the following funding agencies: The National Institutes of Health AR 49635, Doctoral Prize Fellowship from Engineering and Physical Sciences Research Council (EPSRC), UK, the University of Southampton, UK, and the Canadian Institutes of Health Research. MDM is a member of the FRQS Network for Oral and Bone Health Research, and he holds the Canada Research Chair in Biomineralization as part of the Canada Research Chairs program which contributed to the funding of this work. We thank Beate Lanske for the generous dontation of the FGF23 knockout mice and to the Center for Biotechnology and Interdisciplinary

570 Studies Imaging Core at Rensselaer Polytechnic Institute for providing access to micro-
571 computed tomography.

572

References

1. Murshed M, Schinke T, McKee MD, Karsenty G. Extracellular matrix mineralization is regulated locally; different roles of two gla-containing proteins. J Cell Biol. 2004 Jun 7;165(5):625–30.

2. Clarke B. Normal bone anatomy and physiology. Clin J Am Soc Nephrol. 2008 Nov;3(Suppl 3):131–9.

3. Murshed M, McKee MD. Molecular determinants of extracellular matrix mineralization in bone and blood vessels. Curr Opin Nephrol Hypertens. 2010;19(4).

4. Nudelman F, Pieterse K, George A, Bomans PHH, Friedrich H, Brylka LJ, et al. The role of collagen in bone apatite formation in the presence of hydroxyapatite nucleation inhibitors. Nat Mater. 2010 Oct 24;9:1004.

5. Addison WN, Masica DL, Gray JJ, McKee MD. Phosphorylation-dependent inhibition of mineralization by osteopontin ASARM peptides is regulated by PHEX cleavage. J Bone Miner Res. 2010 Apr 9;25(4):695–705.

6. Deng F-Y, Tan L-J, Shen H, Liu Y-J, Liu Y-Z, Li J, et al. SNP rs6265 Regulates Protein Phosphorylation and Osteoblast Differentiation and Influences BMD in Humans. J Bone Miner Res. 2013 May 28;28(12):2498–507.

7. Boskey AL. Bone composition: relationship to bone fragility and antiosteoporotic drug effects. Bonekey Rep. 2013 Jul;2:1–11.

8. Bertazzo S, Gentleman E, Cloyd KL, Chester AH, Yacoub MH, Stevens MM. Nano-analytical electron microscopy reveals fundamental insights into human cardiovascular tissue calcification. Nat Mater. 2013 Apr 21;12:576.

9. McKee MD, Nanci A. Osteopontin at mineralized tissue interfaces in bone, teeth, and osseointegrated implants: ultrastructural distribution and implications for mineralized tissue formation, turnover, and repair. Microsc Res Tech. 1996;33(2):141–64.

10. Thurner PJ, Lam S, Weaver JC, Morse DE, Hansma PK. Localization of phosphorylated serine, osteopontin, and bone sialoprotein on bone fracture surfaces. J Adhes. 2009;85(8):526–45.

11. Thurner PJ. Atomic force microscopy and indentation force measurement of bone. Wiley Interdiscip Rev Nanomedicine Nanobiotechnology. 2009 Nov;1(6):624–49.

12. Sroga GE, Vashishth D. A strategy to quantitate global phosphorylation of bone matrix proteins. Anal Biochem. 2016 Apr;499(2016):85–9.

13. Sroga GE, Vashishth D. Phosphorylation of extracellular bone matrix proteins and its contribution to bone fragility. J Bone Miner Res. 2018 Jul 12;0(ja).

14. Barros NMT, Hoac B, Neves RL, Addison WN, Assis DM, Murshed M, et al. Proteolytic processing of osteopontin by PHEX and accumulation of osteopontin fragments in Hyp mouse bone, the murine model of X-linked hypophosphatemia. J Bone Miner Res. 28(3):688–99.

15. Liu S, Zhou J, Tang W, Jiang X, Rowe DW, Quarles LD. Pathogenic role of Fgf23 in Hyp mice. Am J Physiol Metab. 2006;291(1):E38–49.

16. Boukpessi T, Hoac B, Coyac BR, Leger T, Garcia C, Wicart P, et al. Osteopontin and the dento-osseous pathobiology of X-linked hypophosphatemia. Bone. 2017;95:151–61.

17. Yuan Q, Jiang Y, Zhao X, Sato T, Densmore M, Schüler C, et al. Increased Osteopontin Contributes to Inhibition of Bone Mineralization in FGF23-Deficient Mice. J Bone Miner Res. 2014;29(3):693–704.

18. Harmey D, Johnson KA, Zelken J, Camacho NP, Hoylaerts MF, Noda M, et al. Elevated skeletal osteopontin levels contribute to the hypophosphatasia phenotype in Akp2−/− mice. J Bone Miner Res. 2006;21(9):1377–86.

19. Narisawa S, Manisha YC, Millán JL. In Vivo Overexpression of Tissue-Nonspecific Alkaline Phosphatase Increases Skeletal Mineralization and Affects the Phosphorylation Status of Osteopontin. J Bone Miner Res. 28(7):1587–98.

20. Yadav MC, Huesa C, Narisawa S, Hoylaerts MF, Moreau A, Farquharson C, et al. Ablation of Osteopontin Improves the Skeletal Phenotype of Phospho1−/− Mice. J Bone Miner Res. 2014 May 13;29(11):2369–81.

21. Liu ES, Martins JS, Raimann A, Chae BT, Brooks DJ, Jorgetti V, et al. 1,25-Dihydroxyvitamin D Alone Improves Skeletal Growth, Microarchitecture, and Strength in a Murine Model of XLH, Despite Enhanced FGF23 Expression. J Bone Miner Res. 31(5):929–39.

22. Murali SK, Roschger P, Zeitz U, Klaushofer K, Andrukhova O, Erben RG. FGF23 Regulates Bone Mineralization in a 1, 25 (OH) 2D3 and Klotho-Independent Manner. J Bone Miner Res. 2016;31(1):129–42.

23. Kazanecki CC, Uzwiak DJ, Denhardt DT. Control of osteopontin signaling and function by post-translational phosphorylation and protein folding. J Cell Biochem. 2007 Nov;102(4):912–24.

24. Katayama Y, House CM, Udagawa N, Kazama JJ, Mcfarland RJ, Martin TJ, et al. Casein kinase 2 phosphorylation of recombinant rat osteopontin enhances adhesion of osteodasts but not osteoblasts. J Cell Physiol. 1998 Jul;176(1):179–87.

25. Razzouk S, Brunn J, Qin C, Tye C, Goldberg H, Butler W. Osteopontin posttranslational modifications, possibly phosphorylation, are required for in vitro bone resorption but not osteoclast adhesion. Bone. 2002 Jan;30(1):40–7.

26. Hunter GK, Kyle CL, Goldberg H a. Modulation of crystal formation by bone phosphoproteins: structural specificity of the osteopontin-mediated inhibition of hydroxyapatite formation. Biochem J. 1994 Jun 15;300(3):723–8.

27. Duvall CL, Taylor WR, Weiss D, Wojtowicz AM, Guldberg RE. Impaired angiogenesis, early callus formation, and late stage remodeling in fracture healing of osteopontin-deficient mice. J Bone Miner Res. 2007 Feb;22(2):286–97.

28. Thurner PJ, Chen CG, Ionova-Martin S, Sun L, Harman A, Porter A, et al. Osteopontin

deficiency increases bone fragility but preserves bone mass. Bone. 2010;46(6):1564–73.

29. Poundarik AA, Diab T, Sroga GE, Ural A, Boskey AL, Gundberg CM, et al. Dilatational band formation in bone. Proc Natl Acad Sci. 2012 Nov 20;109(47):19178–83.

30. Zappone B, Thurner PJ, Adams J, Fantner GE, Hansma PK. Effect of Ca2+ Ions on the Adhesion and Mechanical Properties of Adsorbed Layers of Human Osteopontin. Biophys J. 2008 Sep 15;95(6):2939–50.

31. Kaartinen MT, Pirhonen A, Linnala-Kankkunen A, Mäenpää PH. Cross-linking of osteopontin by tissue transglutaminase increases its collagen binding properties. J Biol Chem. 1999;274(3):1729–35.

32. Kaartinen MT, Pirhonen A, Linnala-Kankkunen A, Mäenpää PH. Transglutaminase-catalyzed cross-linking of osteopontin is inhibited by osteocalcin. J Biol Chem. 1997;272(36):22736–41.

33. Kaartinen MT, El-Maadawy S, Räsänen NH, McKee MD. Tissue transglutaminase and its substrates in bone. J Bone Miner Res. 2002;17(12):2161–73.

34. Goldsmith HL, Labrosse JM, McIntosh FA, Mäenpää PH, Kaartinen MT, McKee MD. Homotypic interactions of soluble and immobilized osteopontin. Ann Biomed Eng. 2002;30(6):840–50.

35. Hoac B, Nelea V, Jiang W, Kaartinen MT, McKee MD. Mineralization-inhibiting effects of transglutaminase-crosslinked polymeric osteopontin. Bone. 2017;101:37–48.

36. Cavelier S, Dastjerdi AK, McKee MD, Barthelat F. Bone toughness at the molecular scale: A model for fracture toughness using crosslinked osteopontin on synthetic and biogenic mineral substrates. Bone. 2018;110:304–11.

37. Neame PJ, Butler WT. Posttranslational modification in rat bone osteopontin. Connect Tissue Res. 1996;35(1–4):145–50.

38. Sitara D, Razzaque MS, Hesse M, Yoganathan S, Taguchi T, Erben RG, et al. Homozygous ablation of fibroblast growth factor-23 results in hyperphosphatemia and impaired skeletogenesis, and reverses hypophosphatemia in Phex-deficient mice. Matrix Biol. 2004;23(7):421–32.

39. Camacho NP, Rimnac CM, Meyer Jr RA, Doty S, Boskey AL. Effect of abnormal mineralization on the mechanical behavior of X-linked hypophosphatemic mice femora. Bone. 1995;17(3):271–8.

40. Fantner G, Adams J, Turner P, Thurner P, Fisher L, Hansma P. Nanoscale ion mediated networks in bone: osteopontin can repeatedly dissipate large amounts of energy. Nano Lett. 2007 Aug;7(8):2491–8.

41. Wang Y, Morsali R, Dai Z, Minary-Jolandan M, Qian D. Computational Nanomechanics of Noncollagenous Interfibrillar Interface in Bone. ACS Appl Mater Interfaces. 2020;

42. Gao H, Ji B, Jäger IL, Arzt E, Fratzl P. Materials become insensitive to flaws at nanoscale: lessons from nature. Proc Natl Acad Sci. 2003;100(10):5597–600.

688 43. Zimmermann EA, Barth HD, Ritchie RO. The Multiscale Origins of Fracture Resistance
689 in Human Bone and Its Biological Degradation. JOM. 2012;64(4):486–93.

690 44. Fantner GE, Hassenkam T, Kindt JH, Weaver JC, Birkedal H, Pechenik L, et al.
691 Sacrificial bonds and hidden length dissipate energy as mineralized fibrils separate during
692 bone fracture. Nat Mater. 2005 Aug;4(8):612–6.

693 45. Lai ZB, Wang M, Yan C, Oloyede A. Molecular dynamics simulation of mechanical
694 behavior of osteopontin-hydroxyapatite interfaces. J Mech Behav Biomed Mater.
695 2014;36:12–20.

696 46. Sorensen ES, Hojrup P, Petersen TE. Posttranslational modifications of bovine
697 osteopontin: identification of twenty-eight phosphorylation and three O-glycosylation
698 sites. Protein Sci. 1995 Oct;4(10):2040–9.

699 47. Fantner GE, Oroudjev E, Schitter G, Golde LS, Thurner P, Finch MM, et al. Sacrificial
700 bonds and hidden length: unraveling molecular mesostructures in tough materials.
701 Biophys J. 2006;90(4):1411–8.

702 48. Fisher LW, Torchia DA, Fohr B, Young MF, Fedarko NS. Flexible structures of SIBLING
703 proteins, bone sialoprotein, and osteopontin. Biochem Biophys Res Commun.
704 2001;280(2):460–5.

705 49. Malka-Gibor E, Kornreich M, Laser-Azogui A, Doron O, Zingerman-Koladko I, Harapin
706 J, et al. Phosphorylation-Induced Mechanical Regulation of Intrinsically Disordered
707 Neurofilament Proteins. Biophys J. 2017;112(5):892–900.

708 50. Laser-Azogui A, Kornreich M, Malka-Gibor E, Beck R. Neurofilament assembly and
709 function during neuronal development. Curr Opin Cell Biol. 2015;32:92–101.

710 51. Orgel JPRO, Irving TC, Miller A, Wess TJ. Microfibrillar structure of type I collagen in
711 situ. Proc Natl Acad Sci U S A. 2006 Jun 13;103(24):9001–5.

712 52. Boskey AL, Villarreal-Ramirez E. Intrinsically disordered proteins and biomineralization.
713 Matrix Biol. 2016;52–54:43–59.

714 53. Yuan A, Rao M V, Nixon RA. Neurofilaments and neurofilament proteins in health and
715 disease. Cold Spring Harb Perspect Biol. 2017;9(4):a018309.

716 54. Khalil M, Teunissen CE, Otto M, Piehl F, Sormani MP, Gattringer T, et al.
717 Neurofilaments as biomarkers in neurological disorders. Nat Rev Neurol.
718 2018;14(10):577–89.

719 55. Rittling S, Matsumoto H, McKee M, Nanci A, An X, Novick K, et al. Mice lacking
720 osteopontin show normal development and bone structure but display altered osteoclast
721 formation in vitro. J bone Miner Res. 1998 Jul;13(7):1101–11.

722 56. Yoshitake H, Rittling SR, Denhardt DT, Noda M. Osteopontin-deficient mice are resistant
723 to ovariectomy-induced bone resorption. Proc Natl Acad Sci. 1999 Jul;96(14):8156–60.

724 57. Boskey AL, Spevak L, Paschalis E, Doty SB, McKee MD. Osteopontin Deficiency
725 Increases Mineral Content and Mineral Crystallinity in Mouse Bone. Calcif Tissue Int.

2002;71(2):145–54.

58. Depalle B, McGilvery CM, Nobakhti S, Aldegaither N, Shefelbine SJ, Porter AE. Osteopontin regulates type I collagen fibril formation in bone tissue. Acta Biomater. 2020;

59. Ritchie R, Koester K, Ionova S, Yao W, Lane N, Ager J. Measurement of the toughness of bone: A tutorial with special reference to small animal studies. Bone. 2008 Nov;43(5):798–812.

60. Goldberg HA, Sodek J. Purification of mineralized tissue-associated osteopontin. J tissue Cult methods. 1994;16(3–4):211–5.

61. Knychala J, Bouropoulos N, Catt CJ, Katsamenis OL, Please CP, Sengers BG. Pore geometry regulates early stage human bone marrow cell tissue formation and organisation. Ann Biomed Eng. 2013;41(5):917–30.

62. Andriotis O, Katsamenis OL, Mouzakis DE, Bouropoulos N. Preparation and characterization of bioceramics produced from calcium phosphate cements. Cryst Res Technol J Exp Ind Crystallogr. 2010;45(3):239–43.

63. Ginebra MP, Driessens FCM, Planell JA. Effect of the particle size on the micro and nanostructural features of a calcium phosphate cement: a kinetic analysis. Biomaterials. 2004;25(17):3453–62.

64. Grassinger J, Haylock DN, Storan MJ, Haines GO, Williams B, Whitty GA, et al. Thrombin-cleaved osteopontin regulates hemopoietic stem and progenitor cell functions through interactions with α9β1 and α4β1 integrins. Blood. 2009;114(1):49–59.

65. Christensen B, Schack L, Kläning E, Sørensen ES. Osteopontin is cleaved at multiple sites close to its integrin-binding motifs in milk and is a novel substrate for plasmin and cathepsin D. J Biol Chem. 2010;285(11):7929–37.

66. Sørensen ES, Petersen TE. Purification and characterization of three proteins isolated from the proteose peptone fraction of bovine milk. J Dairy Res. 1993;60(2):189–97.

67. Christensen B, Sørensen ES. Osteopontin is highly susceptible to cleavage in bovine milk and the proteolytic fragments bind the αVβ3-integrin receptor. J Dairy Sci. 2014;97(1):136–46.

68. Boskey AL, Christensen B, Taleb H, Sørensen ES. Post-translational modification of osteopontin: Effects on in vitro hydroxyapatite formation and growth. Biochem Biophys Res Commun. 2012;419(2):333–8.

69. Adams J, Fantner GE, Fisher LW, Hansma PK. Molecular energy dissipation in nanoscale networks of dentin matrix protein 1 is strongly dependent on ion valence. Nanotechnology. 2008 Sep 24;19(38):384008.

Figures

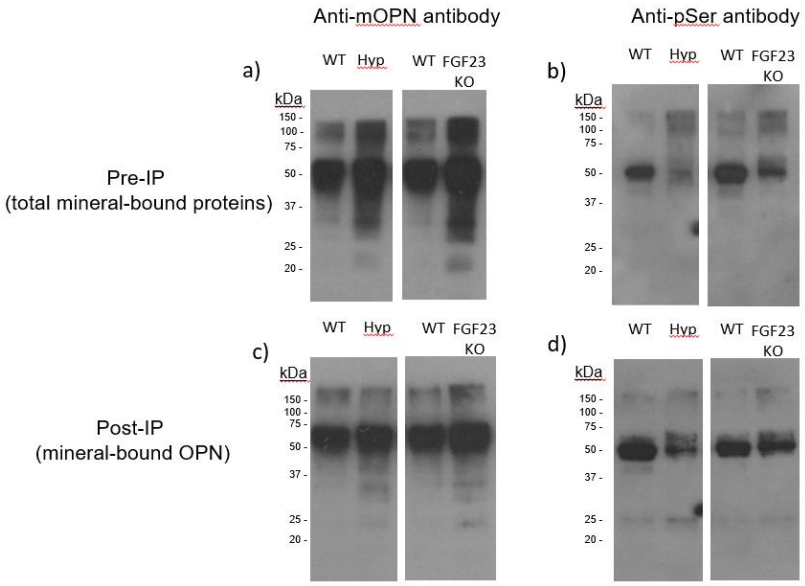

Figure 1: Pre-immunoprecipation (Pre-IP) of mineral-bound OPN (a) and global phosphorylation (b) in protein extracts of long bones from WT, *Hyp* and *Fgf23*$^{-/-}$ mice. Post-immunoprecipation (Post-IP) indicates that despite similar levels of OPN (c), phosphorylation of OPN is reduced in these disease models (d).

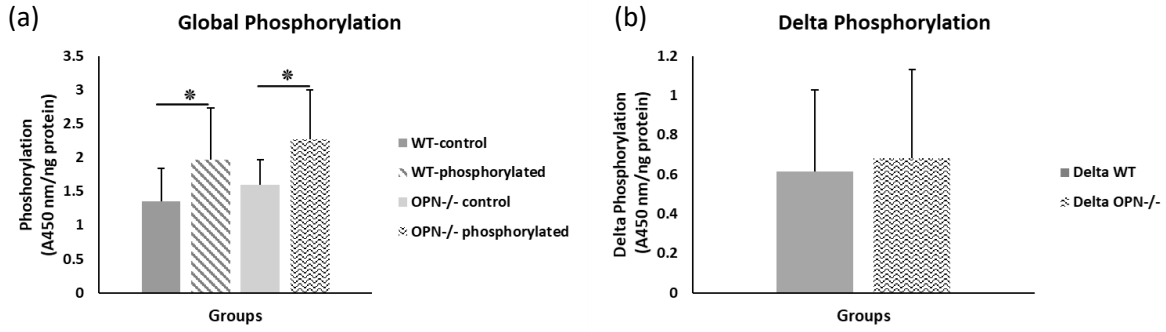

Figure 2: Mean global protein phosphorylation (a) and change in phosphorylation (b) for WT and Opn KO groups. * indicates significance at $p<0.05$ and error bars represent standard deviation.

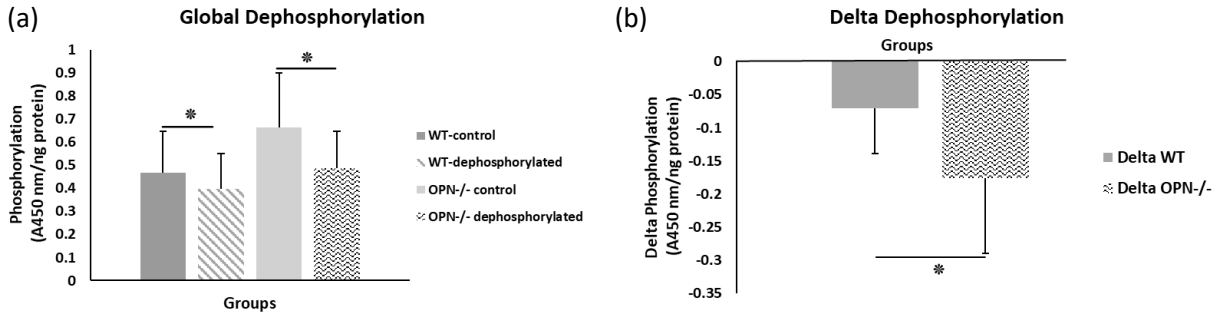

Figure 3: Mean global protein phosphorylation (a) and change in phosphorylation (b) after removal of phosphate groups (dephosphorylation) for WT and Opn KO groups. * indicates significance at $p<0.05$ and error bars represent standard deviation.

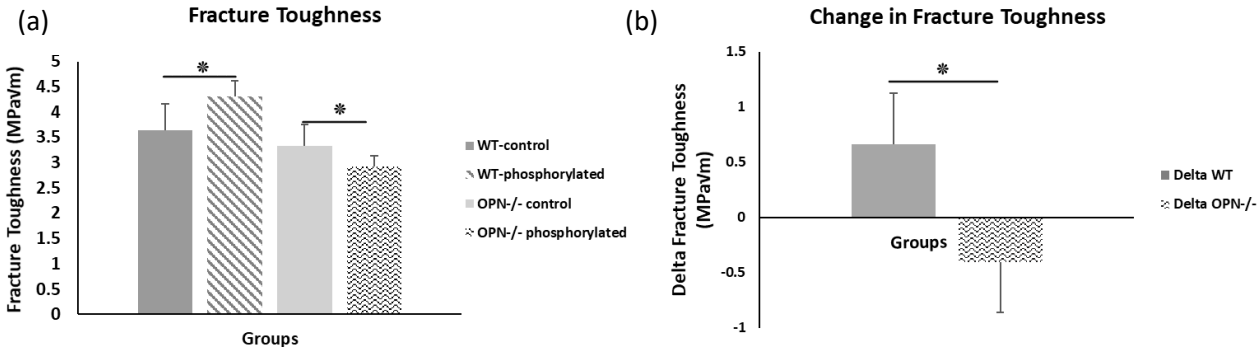

Figure 4: Mean fracture toughness (a) and change in fracture toughness (b) due to *ex vivo* phosphorylation for WT and Opn KO groups. * indicates significance at $p<0.05$ and error bars represent standard deviation.

.

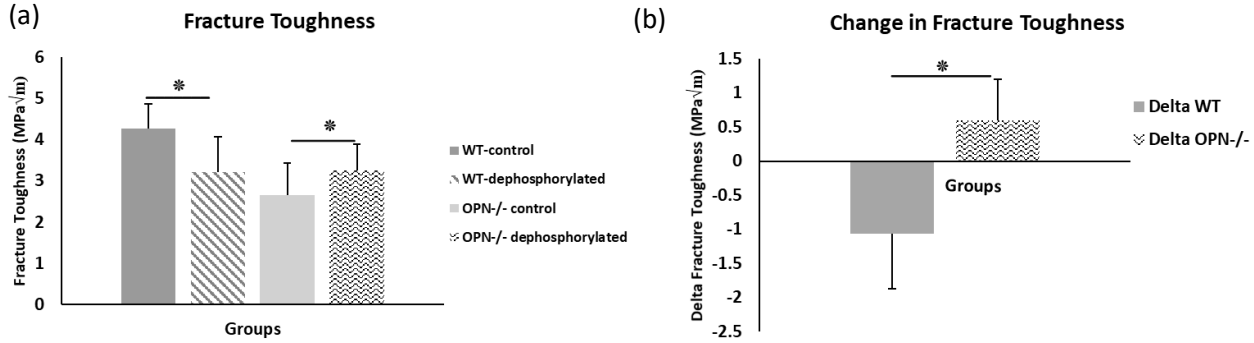

Figure 5: Mean fracture toughness (a) and change in fracture toughness (b) attributable to *ex vivo* dephosphorylation for WT and Opn KO groups. * indicates significance at $p<0.05$ and error bars represent standard deviation.

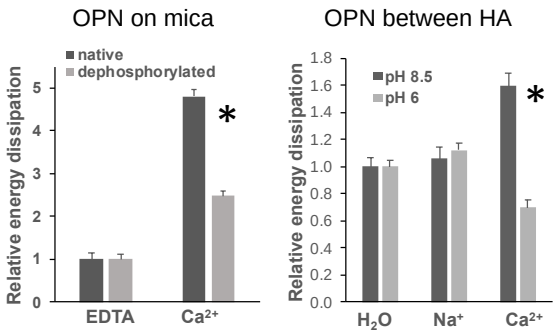

Figure 6: Energy dissipation of OPN networks during AFM-FS experiments. Energies are normalized to dissipation levels in EDTA for OPN deposited on mica and pulled with a pristine AFM tip (pH 7.4) and to dissipation levels in H_2O for OPN deposited on HA and pulled with a HA-functionalized tip. All values are significantly different except OPN between HA, pH 8.5 H_2O vs. Na^+. It should be noted that the relative differences are similar to what is seen for quantitative values, except for EDTA and H_2O levels due to normalization. These values are provided in Supplementary Files 1 and 2. * indicates significance at $p<0.05$ and error bars represent standard error (SE) of the mean.

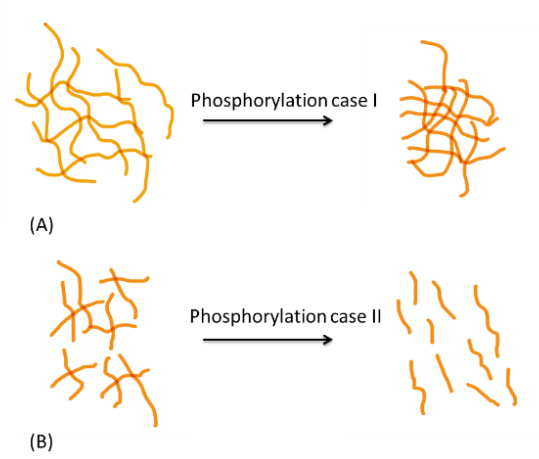

Figure 7: Schematic diagram showing differential effects of phosphorylation on conformation of protein systems. In protein system **(A)**, phosphorylation tends to increase inter- and intrafilament interactions, hence the interfilament distance is reduced. In protein system **(B)**, phosphorylation tends to create interfilament repellant, hence increasing the protein system alignment and inter-filament distance.

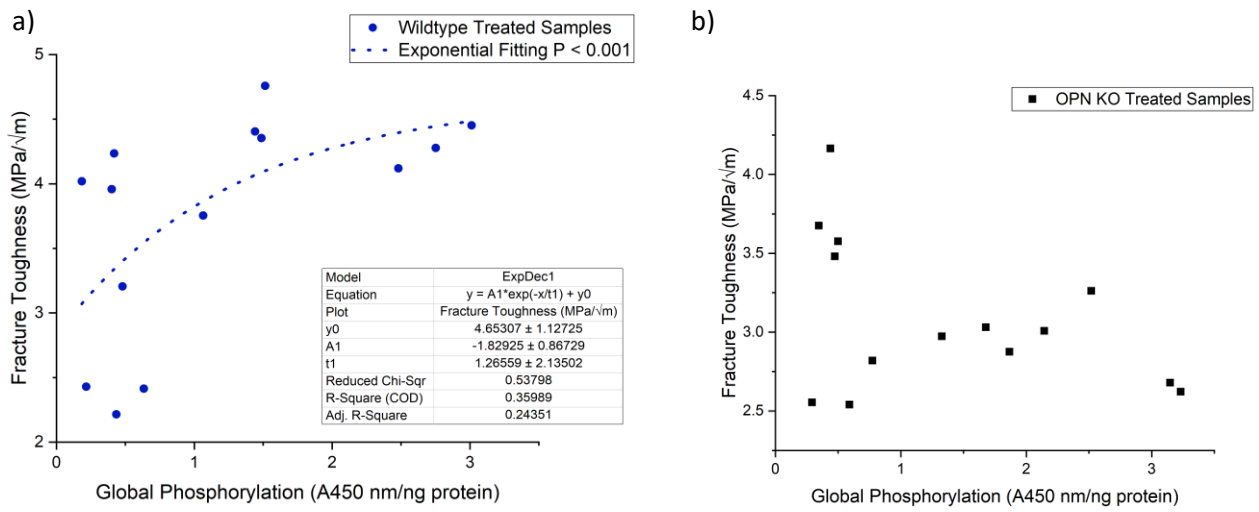

Figure 8: Schematic of the relationship between global protein phosphorylation and fracture toughness of wild-type (a) and Opn KO (b) mice. By continuing the increase in phosphorylation of WT bone, fracture toughness improves exponentially. There is no significant relationship between global phosphorylation and fracture toughness in Opn KO mice following *ex-vivo* phosphorylation and dephosphorylation.

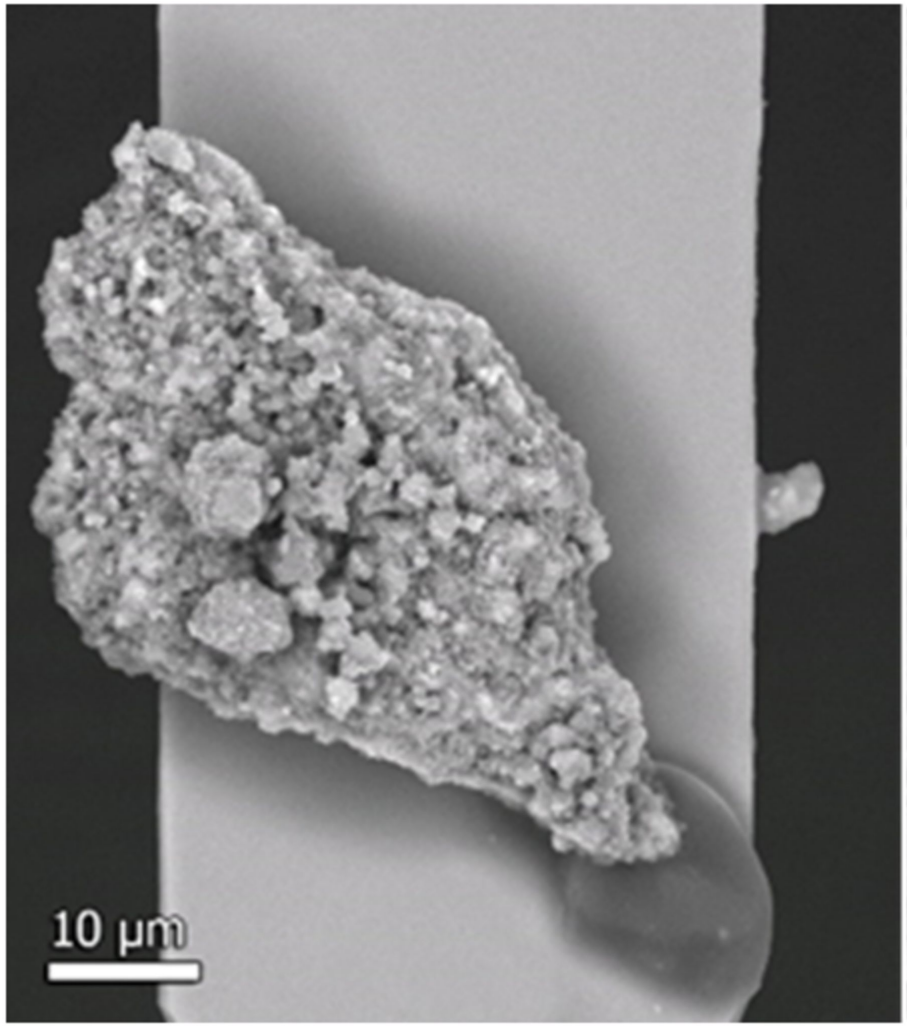
10 µm

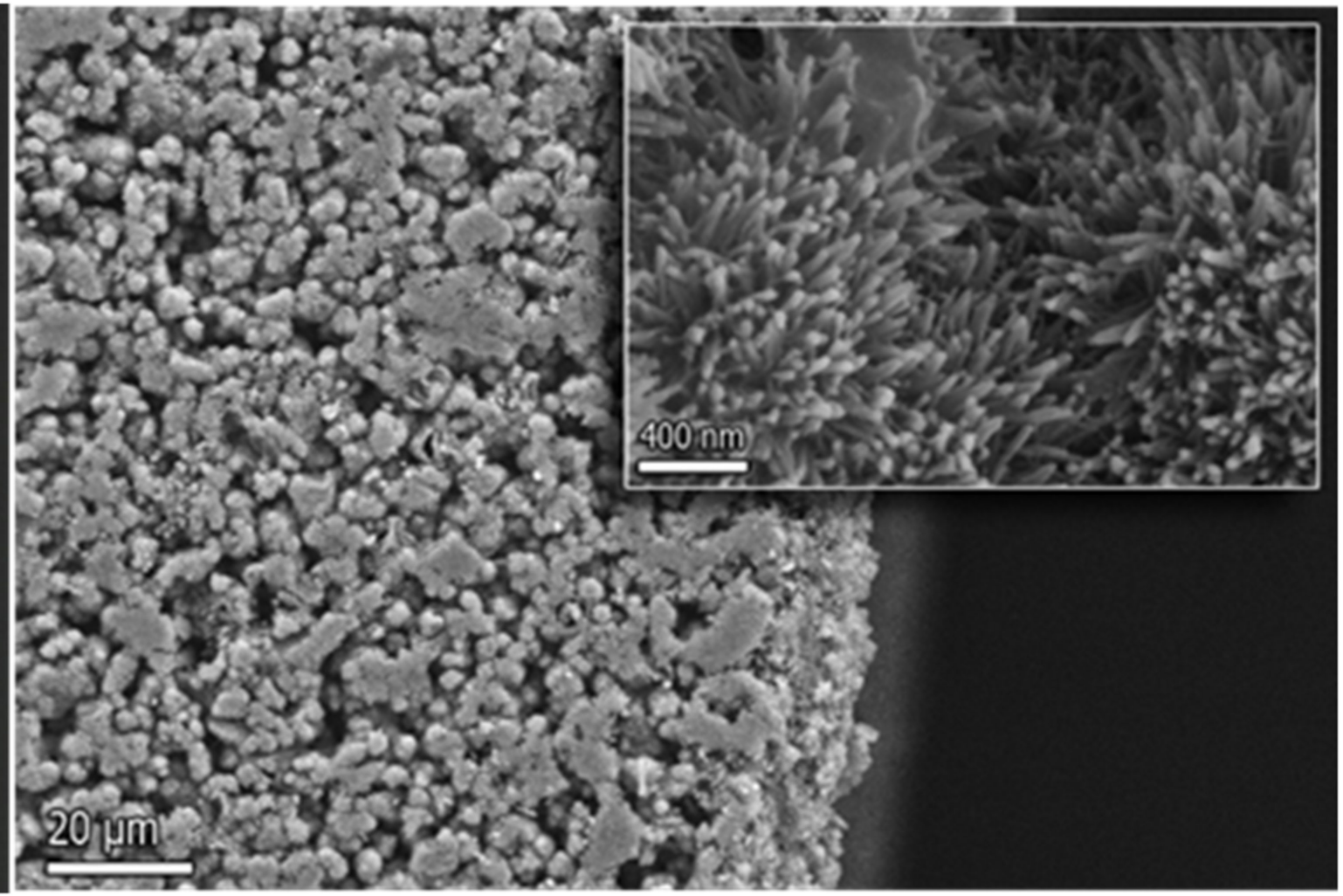
400 nm
20 µm

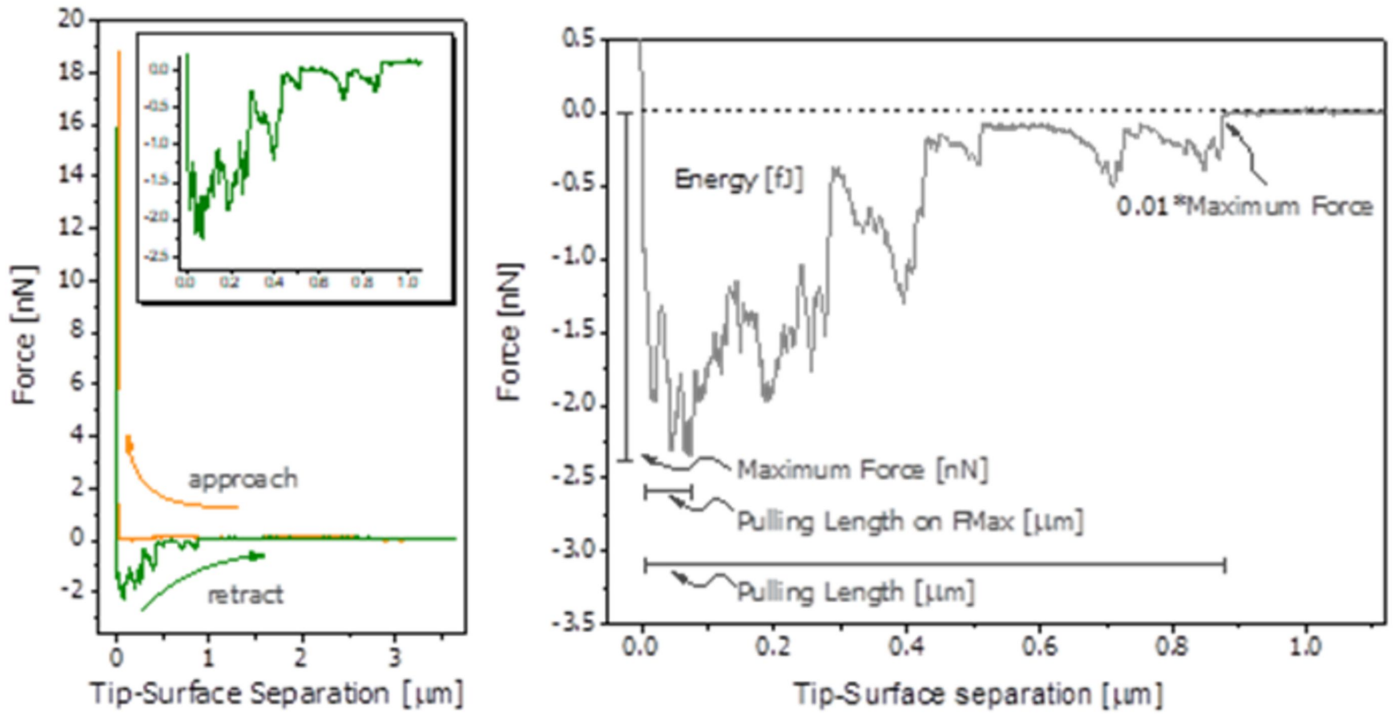
Force [nN]
Tip-Surface Separation [µm]
approach
retract
Energy [fJ]
0.01*Maximum Force
Maximum Force [nN]
Pulling Length on FMax [µm]
Pulling Length [µm]
Tip-Surface separation [µm]

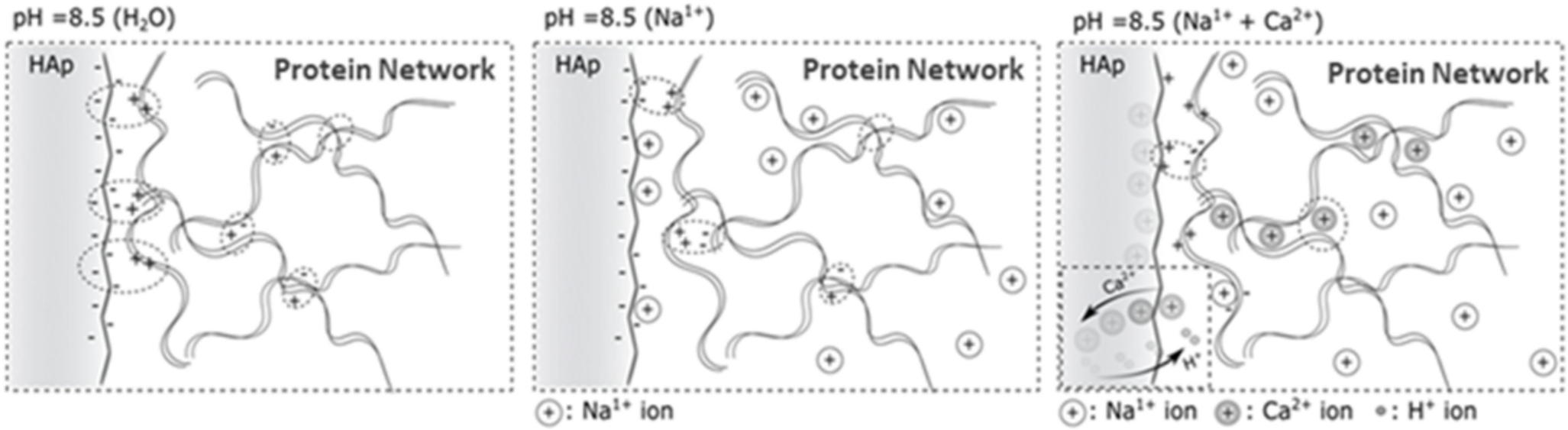
pH =8.5 (H_2O)
HAp
Protein Network
pH =8.5 (Na^{1+})
HAp
Protein Network
: Na^{1+} ion
pH =8.5 (Na^{1+} + Ca^{2+})
HAp
Protein Network
Ca^{2+}
H^+
: Na^{1+} ion
: Ca^{2+} ion
: H^+ ion
pH =6.0 (H_2O)
HAp
Protein Network
: Ca^{2+} ion
pH =6.0 (Na^{1+})
HAp
Protein Network
: Na^{1+} ion
: Ca^{2+} ion
pH =6.0 (Na^{1+} + Ca2+)
HAp
Protein Network
: Na^{1+} ion
: Ca^{2+} ion